

Nanoscale

Accepted Manuscript



This is an *Accepted Manuscript*, which has been through the Royal Society of Chemistry peer review process and has been accepted for publication.

Accepted Manuscripts are published online shortly after acceptance, before technical editing, formatting and proof reading. Using this free service, authors can make their results available to the community, in citable form, before we publish the edited article. We will replace this *Accepted Manuscript* with the edited and formatted *Advance Article* as soon as it is available.

You can find more information about *Accepted Manuscripts* in the [Information for Authors](#).

Please note that technical editing may introduce minor changes to the text and/or graphics, which may alter content. The journal's standard [Terms & Conditions](#) and the [Ethical guidelines](#) still apply. In no event shall the Royal Society of Chemistry be held responsible for any errors or omissions in this *Accepted Manuscript* or any consequences arising from the use of any information it contains.

Connecting Localized DNA Strand Displacement Reactions

Ismael Mullor Ruiz, Jean-Michel Arbona, Amitkumar Lad, Oscar Mendoza,
Jean-Pierre Aimé and Juan Elezgaray.*

CBMN, UMR 5248, CNRS, allée St Hilaire, bât. B14 , 33600 Pessac, France.

E-mail: juan.elezgaray@u-bordeaux.fr

Abstract

Logic circuits based on DNA strand displacement reaction have been shown to be versatile enough to compute the square root of four-bit numbers. The implementation of these circuits as a set of bulk reactions faces difficulties which include leaky reactions and intrinsically slow, diffusion-limited reaction rates. In this paper, we consider simple examples of these circuits when they are attached to platforms (DNA origamis). As expected, constraining distances between DNA strands leads to faster reaction rates. However, it also induces side-effects that are not detectable in the solution-phase version of this circuitry. Appropriate design of the system, including protection and asymmetry between input and fuel strands, leads to a reproducible behaviour, at least one order of magnitude faster than the one observed in bulk conditions.

In 1994, Adleman showed¹ that DNA can be assembled to execute computations at the molecular level. Since then, several computation schemes have been explored, of which DNA strand displacement (SD) reactions and chemical reaction networks are two important

*To whom correspondence should be addressed

examples. In both cases, DNA strands are used to store state. To execute the computation, DNA strands interact through hybridization-dehybridization processes *via* SD reactions. A strand displacement reaction involves three DNA strands: an input strand (I), and output strand (O) and the gate strand (G). In the initial state, output and gate are hybridized forming a duplex (GO). The SD reaction proceeds after the addition of the input strand to the stable GO system. Strand input displaces the output strand leading to the formation of the duplex input-gate (GI) and a free output O . It has been shown² that a SD reaction closely follows a second order reaction of the form:



The binding kinetics of the input and output to the gate can be modulated by the use of short single stranded sequences named 'toeholds'. In ref.², it was shown that SD reactions can be considered as second order reactions, with a kinetic constant directly related to the toehold's length.

Several theoretical and experimental works have shown the possibility to cascade SD reactions in order to perform DNA-based computations. Examples include catalytic reactions networks^{3,4}, logic gates and circuits^{5,6}. Coupling SD reactions to more complex DNA constructions was used in the design of (nano)robots⁷. Possible applications to biosensing devices^{8,9} look particularly promising.

Three basic difficulties have been pointed out in the development of DNA circuits: (i) the characteristic response times of circuits in solution is basically diffusion limited, which for concentrations in the nanomolar range leads to time scales of at least a few hours, (ii) existence of leaky reactions and (iii) unwanted cross talk between different gates. Of these, only point (iii) can be fixed by optimizing the recognition sequences and by using different toeholds.

Our goal in this paper is to consider a possible cure to the intrinsic slowness of diffusion

limited reaction rates. As suggested by several authors^{6,10}, tethering the location of DNA gates on top of a DNA platform makes the reactions between different gates much faster than in solution. Furthermore, reactions between tethered gates are only possible if they are close enough which also solves the problem of unwanted cross-talks. In this work, we use the so called DNA origami platforms^{11,12} as a practical way to enforce the distances between different gates and study the influence of this proximity on the dynamics of a simple example of coupled SD reactions. More precisely, we will focus on amplification circuits, for which one input strand 'generates' several output strands. Amplification circuits are ubiquitous in biological regulation systems. In the context of DNA computing, Qian and Winfree⁶ considered a combination of SD reactions (seesaw gates) with built-in amplification. Besides the three strands of a generic SD reaction, an additional fuel strand (F) was introduced. A seesaw gate can be described by the kinetic equations:



where, for simplicity, all the kinetic constants are set equal to k_s .

The gate strand G is formed by a central sequence g flanked by two 5-nt toeholds (T_I and T_F), thus the gate sequence is of the form $T_I - g - T_F$. The output strand O contains the sequence $T'_F - g'$, which is the complementary sequence of $g - T_F$, and possibly additional bases that can interact with other circuits (in the sequel, primes denote Watson-Crick complementary sequences). In the initial state, the output strand is bound to the gate by the $g - T_F$ segment, leaving T_I as a single strand segment, thus forming a DNA fork. Finally, the input strand I includes the sequence $g' - T'_I$.

In this DNA system, the SD reaction is initiated when the input strand binds to the T_I toehold from the gate and, therefore, displaces the output strand. In bulk conditions, the output can in turn reversibly displace the input. In the confined version considered here,

this displacement is much slower than other SDs, and it will be neglected. Fuel's sequence includes T'_F-g' . Therefore, the fuel strand can bind to the gate through the T_F toehold which, in the initial state of the gate, is occupied by the output. Once the latter is displaced by the input, the fuel can bind to the gate and displace the input, which in turn can act on another gate-output configuration. Overall, the amplification of the input signal is proportional to the relative excess of fuel and GO with respect to input.

In order to mimic the amplification cycle performed by the triad input-gate-fuel, we considered a configuration where a single input is surrounded by four gates, each of which has a neighbouring fuel, with all these sequences immobilized on a DNA origami (Figure 1). The expected behaviour of this device is close to the amplification cycle in bulk conditions: a first SD reaction displaces one output which is transferred to the bulk. The neighbour fuel can displace the input from the gate and the cycle starts again. This cycle is shown in Figure 2.

In ref.¹⁰, a theoretical description of circuits coupling localized SD reactions was given. Besides AND and OR logic gates, the authors also considered a 'fan-out' gate, globally described by the reaction $I \longrightarrow O_1 + O_2 + \dots + O_n$. In the terminology of ref.¹⁰, the arrangement of Figure 1 can be viewed as a 4th degree fan-out, as the input signal is expected to trigger the release of four identical outputs (Figure 3).

In a recent work, Simmel and colleagues¹³ considered a system of two coupled SD reactions, one related to a 'sender' gate, the other to a 'receiver'. Although this paper bears some similarity to ours (coupling of SD reactions with gates tethered to a rectangular DNA origami), the studied systems are quite different as only transmission of a signal was studied. One of the main results of ref.¹³ is the existence of strong leaks when the strands can interact through direct, non diffusion limited, interactions. Clearly, the protection needed to define the initial state of the system is a critical point in the design of coupled SD reactions. Here, we present a SD architecture that allows direct interactions and significantly avoids the leaks inherent to the proximity of tethered strands.

Results

Experimental setting

All the strands participating in the localized amplification circuit (LAC) are attached to a rectangular origami¹² with approximate dimensions 90nm x 60nm (Figure 1). The sequence of each input, gate and fuel strands are formed by an active part, which will be involved in the SD reactions, and a connector elongation, which is used to connect the I , F and G strands to the origami platform. The connector sequence includes a 'foot', 15nt long, that binds directly to strand elongations from the origami (SI), and a single strand poly-T sequence which links the 15-nt 'foot' to the I , G and F strands. This linker is intended to ensure a flexible junction between the foot and the active part of each strand, so that strands are almost free to bind and, at the same time, remain in close proximity (the approximate distance between feet is 5.4 nm). For the linker, we tried 5T and 15T combinations, with a clear advantage for the second choice, as explained below. The structure (Figure 1) of the input, gate and fuel strands is of the form (L is the linker, φ is the foot):

- Input: $(5') g' - T'_I - L - \varphi_I (3')$
- Gate: $(5') \varphi_G - L - T_I - g - T_F (3')$
- Fuel: $(5') \varphi_F - L - T'_F - g' (3')$

We will call this configuration a 'symmetric' configuration, meaning that the active part of input ($g' - T'_I$) contains the same number of nucleotides as the active part of fuel ($T'_F + g'$) with respective toeholds T_I and T_F of equal length. In order to improve the efficiency of the LAC, we have also considered several non-symmetric configurations, where the fuel is of the form $\varphi_F - L - T'_F - g' - T_I^{n'}$. Here, $T_I^{n'}$ denotes the complementary part of the last n nucleotides of T_I . In contrast with the symmetric fuel, the number of complementary bases between asymmetric fuel and gate is higher than that between input and gate. For the sake

of simplicity, in the following we only discuss the asymmetric $\varphi_F - L - T'_F - g' - T_I^{1'}$ fuel, which will be denoted $F + 1$.

As a reporter of the displaced output strand concentration, we use a molecular beacon molecule. It comprises a 4 bp stem and a 10 nt loop with a fluorophore-quencher pair covalently attached to the stem. In the absence of output strand, the quencher molecule largely suppresses the fluorescence of the fluorophore. After the output is displaced and brought to the solution, the loop of the molecular beacon binds reversibly to it, opening the stem and producing a fluorescent signal. The output-loop interaction is largely suppressed when the output is hybridized to the gate (GO state) as the recognition sequence, complementary to the loop, is involved in the GO hybridization. We also verified that other strands (gate and fuel), sharing 5 nt of the recognition sequence, do not trigger the molecular beacon.

To avoid spontaneous SD reaction of the LAC device, both input and fuel need to be initially protected. We designed protection strands $I_{(p,n)}$ and $F_{(p,n)}$ for both the input I and fuel F strands. These protections are partial complementary sequences of respectively I and F , and also bear a 10 nt 'activation' toehold (the toeholds to activate the input and fuel are orthogonal). More precisely, $I_{(p,n)} = T_{(I,n)} - g - T_{Iac}$, where $T_{(I,n)}$ denotes the last n nucleotides of the T_I sequence, and T_{Iac} is the 'activation' toehold. Similarly, $F_{(p,n)} = T_{Fac} - g - T_F^n$, where T_F^n denotes the first n nucleotides of the T_F sequence. Once annealed with their partner (I with $I_{(p,n)}$, F with $F_{(p,n)}$), the input and fuel are inactive. The SD reaction on the LAC device will start therefore immediately after deprotection of I and F . To deprotect them, two activating sequences (I_{act} and F_{act}) were used which contain the complementary sequence of, respectively, T_{Iac} and T_{Fac} . These strands displace the protections, leaving input and fuel in their active state (more precisely, the activator+protection complex is initially bound to the input or fuel only by $5 - n$ base pairs, the k_{off} of detachment being $k_{off} \sim 10^3 \text{s}^{-1}$). Note that the activating sequences contain the active part of the protected strand, but only contain n nucleotides of the toehold (SI). We tried $n = 0, 1, 5$, with a clear advantage for the $n = 1$ option, which will be the only one to be considered here. Using

activators with $n = 5$ is equivalent to adding in bulk input and fuel strands, in which case the bulk and local dynamics are in competition. Once the LAC device is activated and reached a stationary state, we use the input activator with the full 5nt toehold (noted I_{act}^5) as a control to measure the amount of output strands that remain bound to the LAC.

Let us denote $p_n(I)$ (respectively $p_n(F)$) the complex obtained by annealing I and $I_{(p,n)}$ (respectively F and $F_{(p,n)}$). The preparation of the LAC is done in two steps. First, separate annealings are performed to obtain the rectangular origami, $p_n(I)$, $p_n(F)$ and the combination of the gate strand with the output (noted GO). Then, these four components are mixed at 30C, with a large excess (x50) of $p_n(I)$, $p_n(F)$ and GO with respect to the origami. Finally, the system is filtered (SI). The output of this process defines the initial state of the system.

A cartoon of the expected SD reaction pathway is represented in Figure 3. After deprotecting the input, the output strand is displaced to bulk and, as a consequence, the fluorescence signal goes from the background F_b level (Fig.3 A) to F_1 (Fig.3 B). Deprotection of the fuels (Fig.3 C) displaces the input strand, which can successively displace other outputs, the fluorescence signal reaching the asymptotic value $F_4 = F_b + 4(F_1 - F_b)$ (Fig.3 E). Simultaneous deprotection of input and fuel induces a direct fluorescence change from F_b to F_4 . The rest of this paper is devoted to a comparison between this ideal scenario and the experimental, fluorescence signals. As suggested by Figure 3, the operation of the LAC could, in principle, also be followed by Atomic Force Microscopy (AFM). However, because the relative distances between different gates is ~ 5 nm, and the linker between gates and the origami is quite flexible, this imaging turns out to be quite difficult. As suggested by the last panel of Figure 3, the LAC final state should be characterized by a distinctive cross-shaped pattern. Figure 2 of SI shows the result of AFM imaging on the LAC's final state. The binding of gates to the origami platform appears to be quite successful. A more detailed view of the LAC structure shows two diffuse 'blobs', separated by 20 nm, a distance compatible with that separating two fuel gates on the model Figure 1. We will further comment this result in the discussion section.

Protection is a necessary ingredient to define the initial state of the system in a meaningful way. We found that it needs to be adapted to each particular system to avoid leak reactions. Figure 4 compares the fluorescence signals obtained with the initial state of the system for the 5T and 15T elongations and the $(I_{(p,0)}, F_{(p,0)})$ protections: leaks are apparent in the 5T system and, at least in the time scale of the experiment, not in the 15T case (in the 5T case, ~ 150 s are needed to reach 10% of the maximum expected fluorescence, ~ 1800 s in the 15T case). The $(I_{(p,1)}, F_{(p,1)})$ protections seem, in turn, to suppress largely the leaks in the 5T system with the disadvantage of slowing down the activation process. In the following, we will focus on the 15T system.

Checking the origin of fluorescence

Strands participating in the LAC can interact in various ways. The faster dynamics corresponds to the intra-origami, non diffusion-limited interactions. However, inter-origami as well as interactions between unfiltered gates cannot be excluded. As mentioned above, the final preparation step of the localized amplification circuit is a filtration. This ensures that most of the strands with size below the filter cutoff (staples and unattached GO, $p_0(I)$ and $p_0(F+1)$ constructions) are not present after filtration. In order to quantify the effect of potential leftover, unbound gates, we performed three experiments, with (respectively) 0, 1 and 2 pmol of scaffold M13mp18, 5 fold excess of staple strands and, for the three experiments, the same amount (50 pmol) of protected strands ($p_0(I)$ and $p_0(F+1)$) and GO gates. After incubation, the same purification process was applied to these systems. Notice that quantities are given in pmol: because all the reactants are mixed in a 0.5 mL cuvette, the equivalent concentrations in nM are obtained by a multiplication by 2.

In Figure 5 are shown the fluorescence signals obtained in these three experiments. The first part of the dynamics ($0 \leq t \leq 1500s$) corresponds to the activation of the LAC. The second corresponds to the addition of I_{act}^5 . The fluorescence signals are clearly correlated to the M13mp18 concentration. This signal is negligible in the absence of origamis. This obser-

vation shows that the fluorescence signal arises mainly from the strands initially attached to the origami platform and not from the leftover, incorrectly filtered unbound strands. Notice that these results do not exclude inter-origami interactions. Those can be shown to be slow compared to the much faster, non diffusion limited intra-origami SD.

The global yield of the reaction is the ratio between the asymptotically observed fluorescence after deprotection of input and fuel and the maximum expected fluorescence corresponding to all the output strands bound to the origamis. The latter can be estimated by addition of a large quantity of I_{act}^5 . In this way, all the output strands that have not been displaced by the tethered inputs can be completely transferred to bulk. As shown in Figure 5, the overall yield of the reaction was around 50%. This yield was highly reproducible between different runs of the same experiment. Two extreme situations could explain this result: either half of the tethered LAC are not well formed, as a result of non efficient annealing, or well formed LACs do not work properly, for instance fuel is not 100% efficient to displace the input.

Comparison with the non scaffolded seesaw gate

Let us now consider the influence of tethering the gates to the origami. One solution was prepared by mixing 2 pmol of $p_0(I)$, 8 pmol of both GO and $p_0(F+1)$ (no filtering was applied to this mixture). The system was activated by the simultaneous addition of I_{act} and F_{act} . The SD was monitored and compared to the SD reaction on a LAC device, prepared by mixing 2 pmol of rectangular origamis with a large excess of $p_0(I)$, GO and $p_0(F+1)$, then filtering. The results, reported in Figure 6, show that the response time scale is at least one order of magnitude faster when the LAC is attached to the origami. As discussed below, this speed-up only sets a lower bound to the LAC dynamics because at least two reactions (fluorescence reporting and input-fuel activation) are limiting factors for the measurement of the speed-up.

Influence of the asymmetry of the seesaw gate.

In the original formulation of the seesaw gate, Qian and Winfree designed the input and fuel strands with symmetric structures. This considerably simplifies the design and quantitative description of the coupling between different gates. However, when seesaw gates are tethered, symmetry has a drawback: once the output has been displaced, the fuel seems to displace only part of the inputs. Figure 7 compares the dynamics obtained with the symmetric and asymmetric versions of the fuel. In the symmetric case, the expected 1:3 behaviour (the ratio between the output observed after activating, respectively, the input and the fuels, see Figure 3) is actually close to a 1:1 behaviour (the amount of fluorescence produced after the activation of the input and fuel are very similar). One way to circumvent this problem is to lengthen by 1nt the fuel strand. As a consequence, because $\Delta G(G + F + 1) < \Delta G(G + I)$, the equilibrium between the $G + F + 1$ and $G + I$ complexes is shifted towards $G + F + 1$ and the 1:3 behaviour is recovered (Figure 7).

Discussion

In bulk conditions, seesaw gates can be modelled as a set of coupled, reversible bimolecular reactions given by equations 2 and 3. The activation and reporting processes can be written as:



Here, $p(I)$ denotes input strand hybridized with input protection (sequences are given in SI), pI_{act} the 'waste' double strand obtained by hybridizing I_{act} and input protection, f is the opened beacon hybridized to the output O , and b is the beacon in the 'closed', quenched state.

In contrast, LAC behave as unimolecular processes:



where λ_n denotes the concentration of LAC with n output strands, the initial state being λ_4 (no distinction is made between different configurations of the LAC for $n < 4$) and $p(\lambda_4)$ is the concentration of LAC with n *protected* fuel and input strands. Note that eq. 7 is a global description of several processes illustrated in Figure 2: strand displacement of output from gate, then strand displacement of input bound to gate strand by fuel. As we demonstrate below, these processes are fast compared to diffusion limited reactions and can be lumped together in a single equation 7.

The reporting process involves an equilibrium between the closed and open configuration of the molecular beacon. Fitting (Figure S1) of the beacon response to the addition of output strand yields $k_{\text{rep}} = 4.4 \times 10^4 M^{-1} s^{-1}$, $q_{\text{rep}} = 0.09 s^{-1}$.

The activation process can be modelled as an irreversible strand displacement reaction, with $k_{\text{act}} \sim 10^6 M^{-1} s^{-1}$. Because we have considered activation conditions with a large excess (100 nM concentration, that is 100 fold excess) of the activator strand, the characteristic time of activation is 10 s, which is comparable to the reporter time response. Therefore, activation can be considered as instantaneous.

In order to push further the analysis and compare LAC dynamics with bulk strand-displacement reactions, it will be helpful to derive a simple biophysical model for strand displacement reactions between tethered strands. In ref.², Zhang and Winfree studied thoroughly the kinetics of the strand displacement reaction under bulk conditions and concluded that it can be modelled as a three step process: toehold binding, branch migration and toehold exchange. Only the first of these steps involves intermolecular interactions. In bulk conditions, toehold binding is a diffusion limited, bimolecular process whereas in tethered

conditions, the binding is expected to be faster and governed by a unimolecular reaction rate. Following previous analysis¹⁰, we approximate the kinetic constant of toehold binding under tethered conditions k_t as

$$k_t = k_b c^*,$$

where k_b is the bulk constant (with units $\text{M}^{-1}\text{s}^{-1}$), and c^* is an effective concentration to be computed. To get an estimate of c , we follow the approach of Genot et al.¹⁴. The analysis is as follows: toehold binding requires the encounter of two single strands. Let us assume that a volume of lateral size a determines the region where encounters are successful. Each of the two single strands is attached to the end of a double strand helix, 15 bp long, which can be assimilated to a stiff rod. Let $p(a)$ be the probability that the two single strands coincide inside the reaction volume. Then,

$$c^* = p(a) 10^{-3} N_a^{-1} a^{-3}$$

where N_a is the Avogadro number and the factor 10^{-3} ensures that the units of c^* are M.

If L is the distance between the foot of the two gates, and l is the length of the foot, there are $\pi\sqrt{l^2 - L^2/4}/a$ small reaction volumes where successful encounters can take place. For each of these points, the probability of presence of the end of the rod is $a^3/(2\pi l^2 a)$ (that is, the ratio between the volumes of the reaction volume and the spherical shell of radius l and width a). Finally,

$$p(a) = \left(\frac{a^3}{2\pi l^2 a} \right)^2 \pi \sqrt{l^2 - L^2/4} \frac{1}{a},$$

and

$$c^* = \frac{1}{4\pi l^4} \sqrt{l^2 - L^2/4} \frac{1}{10^3 N_a}.$$

Notice that this expression is both independent of the size a and correctly predicts a null effective concentration when $L > 2l$ (to be compared with section 3.1 of ref.¹⁰). Notice also that this analysis does not take into account the influence of the additional flexibility of the

T5 or T15 junction, which is to be included inside the reaction volume.

For a typical value of $k_b = 5 \times 10^6 \text{M}^{-1}\text{s}^{-1}$, $k_t = 5000\text{s}^{-1}$, which is much faster than both the response time of the molecular beacon and the branch migration (typical time scale $\sim 1\text{s}$, see ref.², although others¹⁵ report faster processes, in the 10^{-1}s range). We then conclude that SD reactions in LAC are essentially dominated by the branch migration random walk. This unimolecular process sets a lower limit to the time response of any LAC.

The same reasoning can be applied to 'leaky' reactions, in particular blunt-end SD reactions that can be ignored in bulk. Two of these leaks are of interest: (i) binding of the protected input to the unprotected T_I toehold, and (ii) fuel strand displacing the output still attached to the gate strand. From the previous argument and taking into account the measured¹⁴ blunt-end strand displacement $k_{blunt} = 0.8\text{M}^{-1}\text{s}^{-1}$, the 'tethered' leak reaction constant can be expected $\sim 10^{-3}\text{s}^{-1}$. This sets an upper bound to the duration of the experiment beyond which leaks could be important.

With these time scale estimates in mind, the behaviour of the LAC can be described as follows. In the protected, initial state, toehold binding by the protected input is strongly disfavoured but not completely absent: it corresponds to a blunt end toehold binding, with a characteristic time scale $\sim 10^3\text{s}$. This estimate does not take into account the hindrance caused by the attachment of the initially free toehold T_I : the fact that protection is effective for the 15T LAC and not for the 5T LAC illustrates this point. We have shown that protection can be increased by 'overprotecting' T_I ($p_1(I)$ experiment in Figure 4).

The observed LAC dynamics involves the beacon response, the activation process and the SD reactions themselves. In order to get an estimate of the rate of output production by the LAC, we analysed two experiments, with the same initial conditions: in the first, only the input is activated, while in the second, both the input and fuel were activated. For the first experiment, a fitting (Figure S4) to the kinetic model eq. (6) yields a lower bound for the kinetic constant $k > 0.5\text{s}^{-1}$. This estimate can be refined to $k > 5\text{s}^{-1}$ by comparison with the second experiment (Figure S5), for which we postulate a cascade of reactions given

by eq. 6, with a single kinetic constant k . The modelling cannot go further as the time response of the molecular beacon is slower than the largest characteristic time involved in localized SD. Notice however that this estimate is in agreement with a previous estimate of the branch migration time scale¹⁵ which has been shown to control the LAC dynamics.

Conclusions

We have shown that localized amplification circuits can be synthesized by tethering DNA strands to origamis. The resulting system can be seen as a set of seesaw gates, a la Qian and Winfree, attached to rigid rods, that can interact in a way that is not controlled by translational diffusion but only rotational diffusion of the rods. As expected, the resulting dynamics is much faster than previously measured diffusion limited amplification circuits. In turn, tethering enhances any blunt end (no toehold) SD reaction which need to be taken into account in the design of localized circuits. We have shown that a well defined initial state can be obtained when appropriate protections prevent the active part of the strands to interact with each other. The observed leaks remain small in the time scale of the fast, localized interactions inside LAC.

Overall, the LAC is at least one order of magnitude faster than the equivalent bulk version although it is conceivable to improve this ratio by adapting the reporting method. Alternative solutions with no intermediates (such as fluorophore and quencher incorporated in the output and gate) could be studied, with the drawback of increasing the background noise. Elasticity of the attachment seems to play an important not only on the dynamics but also on the protection of the initial state. Further studies will be needed to elucidate this point.

The fact that the yield is below 50% is a recurrent result of this work. Because external, diffusion limited, activation of all the gates is possible (addition of the I_{act}^5 strand), this upper bound points to an intrinsic limitation of the current strategy. The 5T or 15T linkers provide

with flexibility but, at the same time, bring additional crowding, which could explain the inability of part of the input gates to displace the output (the same remark applies to the fuel action). This seems to be confirmed in part by AFM imaging: only two of the expected four motifs were observed in the LAC's final state. Bringing together two stiff rods (the foot of each gate) is also influenced by the strength of electrostatic interactions. In this sense, the effect of salt and probably the concentration of divalent cations is another open possibility to be explored.

This work should be considered only as a first step towards the design of more complex DNA circuits. Several paths could be envisaged. Reif and coworkers¹⁰ considered sets of hairpin structures and showed that, in the framework of dual rail logic, any boolean function could be computed. Assembling hairpin structures in the way we arranged linear structures is an open possibility presumably more challenging than the present one. This stems from the fact that hairpin structures have an alternative, intermolecular assembly pathway.

Materials and Methods

System Preparation

DNA oligonucleotides used in this work (staples, M13mp18 and molecular beacon) were purchased from Sigma-Aldrich. Concentrations were determined from the absorbance at 260 nm (Nanodrop Thermo Scientific) using the extinctions coefficients given by the oligonucleotide provider. Origami staples (desalted quality) were used with no further purification, gate strands were HPLC purified. All DNA oligonucleotides were stored in water at -20°C .

All experiments were done on TAE buffer (Tris acetate-EDTA, purchased as 10x stock from Sigma-Aldrich) with 12.5 mM magnesium acetate. DNA origamis were annealed with two different temperature ramps, from 90 °C to 60 °C in 1 h, from 60 °C to 20 °C in 2 h. The concentration excess of staples versus M13 virus was 5x. In a separate annealing (90 °C to 20 °C in 1 h), protected versions of the input and fuel as well as the GO complex were prepared,

with a 1.2 : 0.8 ratio in concentrations between (protection,output) strands and (input, fuel, gate) strands. No further purification was used to remove unbound single strands. The final system (origami with the different gates attached) was obtained by incubating, for 1 h at 30 °C , origamis with 10 fold excess of p(I), p(F) and GO complexes. Finally, the system was purified using Amicon Ultra-0.5 mL 100K filters (30' filtration at 13000rpm).

Spectrofluorimetry Studies

Fluorescence measurements were done in a Fluoromax-4 (Horiba) using 0.5 mL quartz cells with 1cm pathway. For all the experiments, excitation was at 494 nm (5nm slit) and emissions recorded at 520 nm (5 nm slit). The temperature was controlled and set to 20°C . Beacon concentration was 20 nM. Data points were collected every 60 s, with an integration time of 0.1 s and antibleaching control. The activation of the strands, by addition of 5 μ L of 10 μ M solutions of the activators, was done by quickly pipetting and gently shaking the cell, to avoid as much as possible bubble formation. Despite this, artificial 'jumps' in the fluorescent signal were observed following the activation. Those were removed by assuming continuity of the signal.

Fluorescence Normalization

Prior to any experiment, a measurement of the fluorescence levels of 2 nM and 4 nM of output strand solution was used to calibrate the beacon reporter. Fluctuations of the order of 10% were observed between different runs of the same system.

References

1. Adleman, L. Molecular Computation of Solutions to Combinatorial Problems. *Science* (1994) **266**, 1021-1024.

2. Zhang, D.Y.; Winfree, E. Control of DNA Strand Displacement Kinetics Using Toehold Exchange. *J. Am. Chem. Soc.* (2009) **131**, 17303-17314.
3. Zhang, D. Y.;, Turberfield, A. J.; , Yurke, B.; Winfree, E. Engineering Entropy-Driven Reactions and Networks Catalyzed by DNA. *Science* (2007) **318**, 1121-1125.
4. Yin, P.; Choi, H.M.; Calvert, C.R.; Pierce, N.A. Programming Biomolecular Self-Assembly Pathways. *Nature* (2008) **451**, 318-322.
5. Seelig, G.; Soloveichik, D.; Zhang, D.Y.; Winfree, E. Enzyme-Free Nucleic Acid Logic Circuits. *Science* (2006) **314**, 1585-1588.
6. Qian, L.; Winfree, E. Scaling Up Digital Circuit Computation with DNA Strand Displacement Cascades. *Science* (2011) **332**, 1196-1201.
7. Sherman, W.B.; Seeman, N.C. A Precisely Controlled DNA Biped walking Device, *Nano Lett.* (2014) **4**, 1203-1207.
8. Li, B.; Ellington, A.D; Chen, X. Rational, modular adaptation of enzyme-free DNA circuits to multiple detection methods. *Nucl. Ac. Res.* (2011) **39**, e110.
9. Dirks, R.M; Pierce, N.A. Triggered Amplification by Hybridization Chain Reaction. *PNAS* (2004) **101**, 15275-15278.
10. Chandran, H.; Gopalkrishnan, N.; Phillips, A.; Reif, J. Localized Hybridization Circuits. In *DNA Computing and Molecular Programming*; Cardelli, L., Shih, W., Eds.; Springer: berlin, 2011; Vol. 6937, pp 64-83.
11. Rothmund, P.W.K. Folding DNA to Create Nanoscale Shapes and Patterns. *Nature* (2006) **440**, 297–302.
12. Ke, Y.; Lindsay, S.; Chang, Y.; Liu, Y.; Yan, H. Self-Assembled Water-Soluble Nucleic Acid Probe Tiles for Label-Free RNA Hybridization Assays. *Science* (2008) **319**, 180.

13. Teichmann, M.; Kopperger, E.; Simmel, F. C. Robustness of Localized DNA Strand Displacement Cascades, *ACS Nano* (2014) **8**, 8487-8496.
14. Genot, A.J.; Zhang, D.Y.; Bath, J.; Turberfield, A.J. Remote Toehold: A Mechanism for Flexible Control of DNA Hybridization Kinetics. *J. Am. Chem. Soc.* (2011) **133**, 2177-2182.
15. Srinivas, N.; Ouldrige, T.E.; Sulc, P.; Schaeffer, J.M.; Yurke, B.; Louis, A.A.; Doye, J.P.K.; Winfree, E. On the Biophysics and Kinetics of Toehold-Mediated DNA Strand Displacement. *Nucl. Ac. Res.* (2013) **41**, 10641-10658.

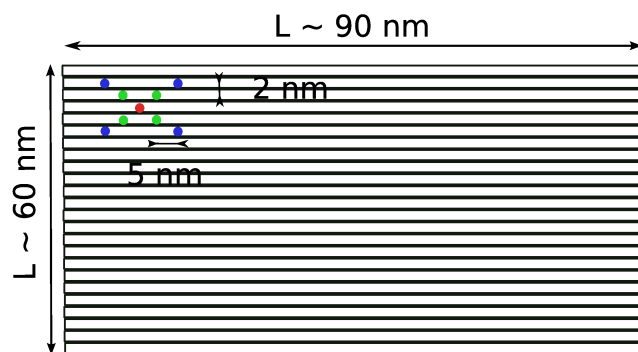
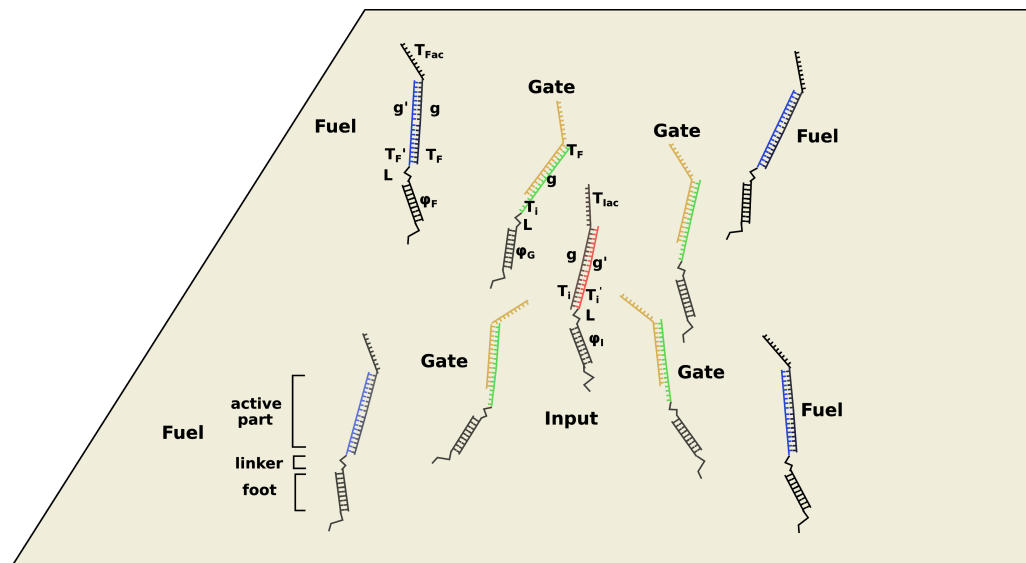


Figure 1: Initial configuration of the nine partially hybridized gates that constitute the localized amplification circuit. The upper panel is a schematic representation of the relative position of the nine gates, all of them being attached to a rectangular origami (lower panel). Color codes represent the function of each active strand: green (gate), red (input), blue (fuel), brown (output). The foot of each strand is in black, as are the protections of input and fuel.

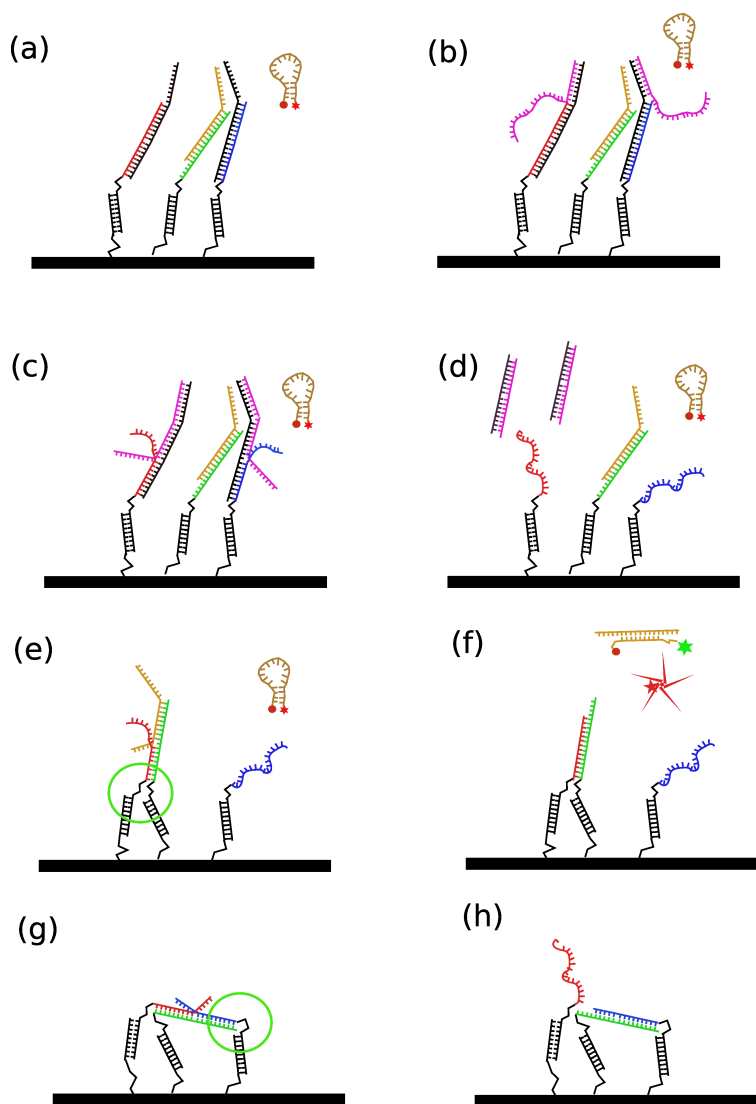


Figure 2: Ideal functional steps of an amplification cycle for gates tethered to a rectangular origami. Same representation as in Figure 1. In the sake of simplicity, only the three gates involved in an elementary step of the amplification cycle have been represented. (a) initial, inactive state. (b) Activator strands (purple) bind to the activator toeholds of input and fuel, respectively. (c) Activator strands initiate SD to remove the protections. (d) Protections have been removed by activator strands, leading to 'waste' double strands and activated fuel and input. (e) Input initiates SD to remove the output (brown). (f) Output has been completely removed from gate. It binds to a molecular beacon, leading to a fluorescent signal. (g) Fuel starts SD to remove the input. (h) Fuel has displaced the input, which is ready to displace another output, beginning a new cycle. Green circles point to possible steric clashes.

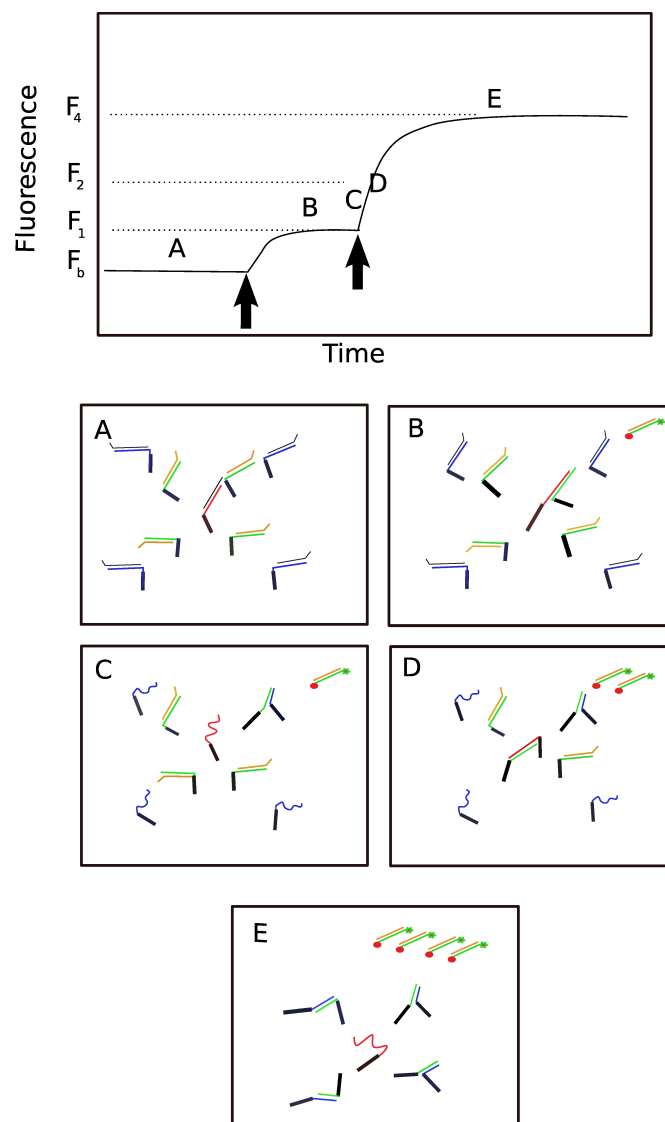


Figure 3: Ideal functional steps of an amplification cycle for gates tethered to a rectangular origami, compared to the corresponding fluorescence signal. Each strand, respectively input (red), fuel (blue) and gate (green) is attached (black thick line) to the origami. Weavy lines indicate single strands, straight lines double stranded segments. Brown segments represent output strands which, once detached from the gate, open the molecular beacon. (A) initial, inactive state. Corresponds to the F_b background signal. (B) Protection has been removed from the input (first vertical arrow in the fluorescence panel), which displaces one output. This corresponds to the F_1 fluorescence level. (C) Fuels become unprotected (second vertical arrow in the fluorescence panel). (D) One fuel strand displaces the input which in turn liberates another output. Fluorescence signal is $F_2 = F_b + 2(F_1 - F_b)$. (E) Ideally, this process continues until all the outputs have been removed from the origami platform. The final fluorescence signal is $F_4 = F_b + 4(F_1 - F_b)$. When input and fuel are activated simultaneously, fluorescence goes directly from F_b to F_4 .

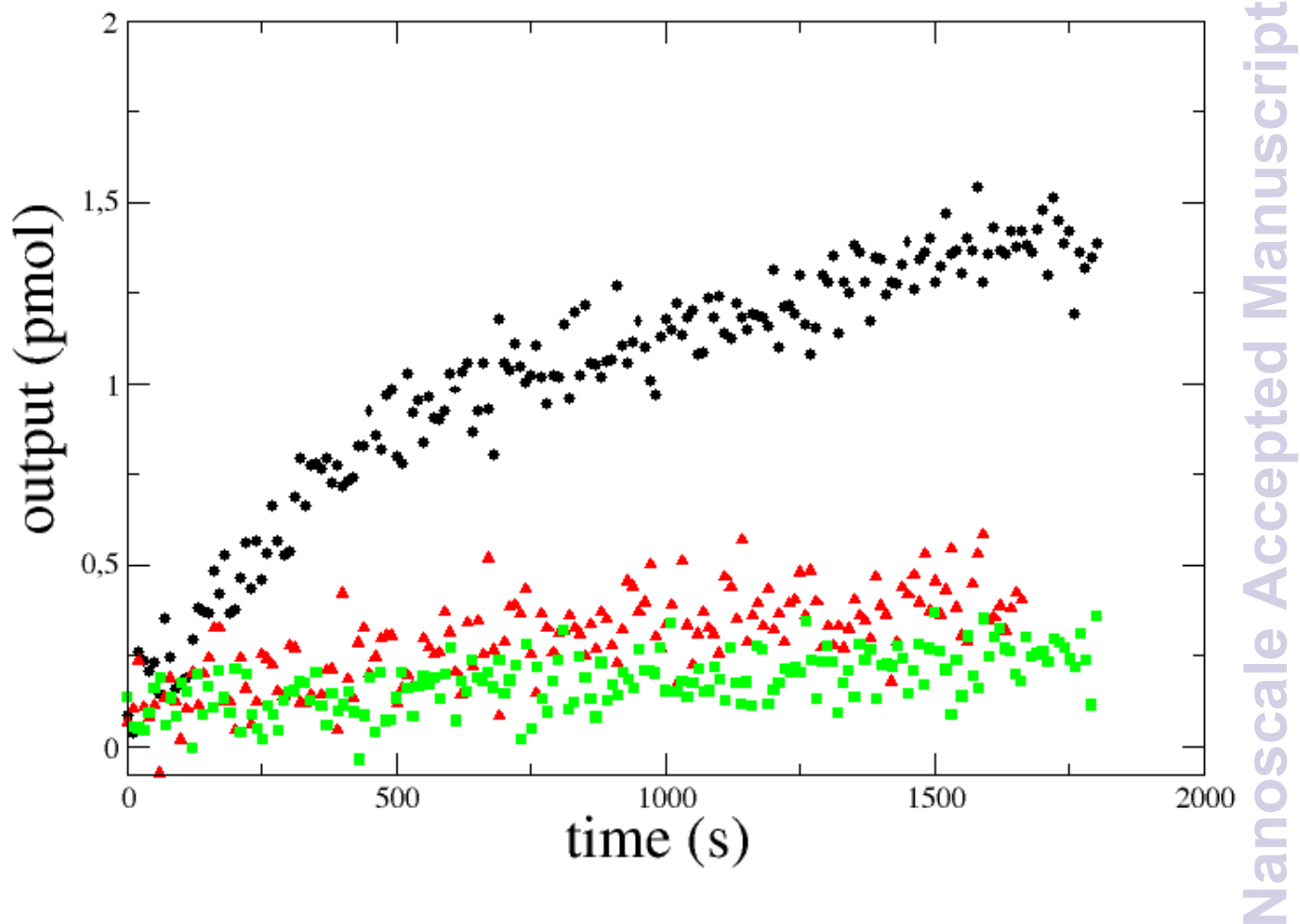


Figure 4: Comparison of the fluorescence observed with different 'protected' states: dots: $p_0(I,15T)$, triangles ($p_0(I,15T)$), squares ($p_1(I,5T)$). The 15T flexible linker seems to contribute to the protection of the initial state.

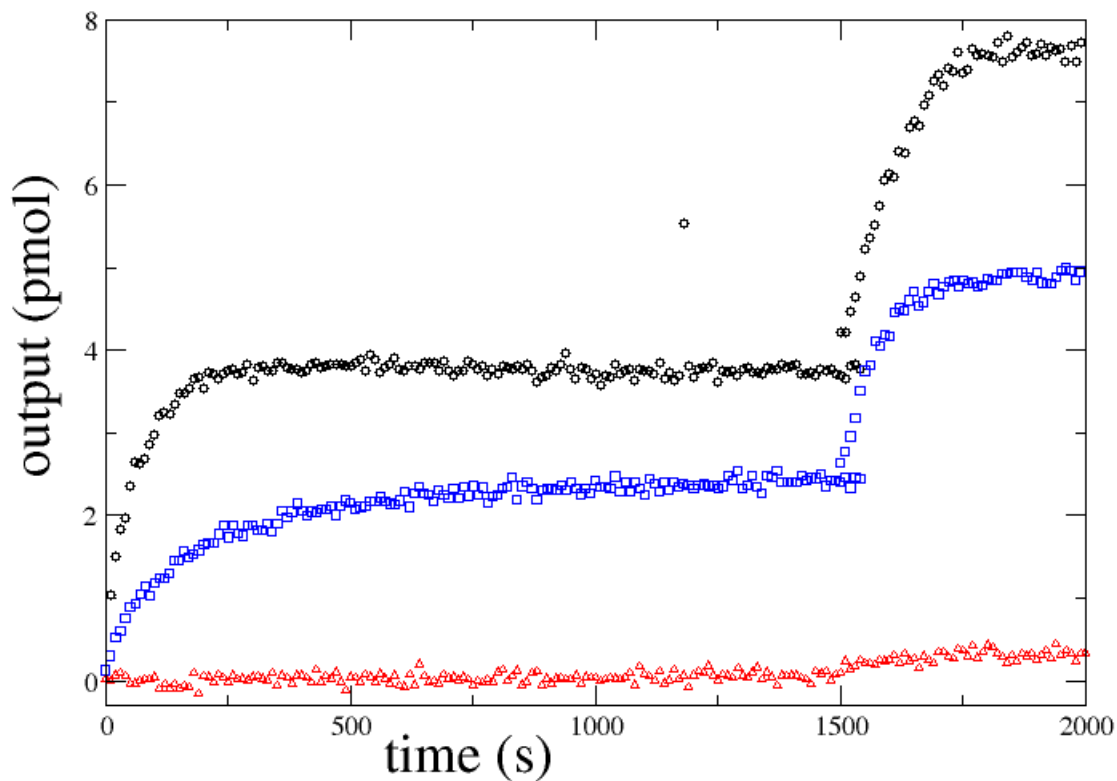


Figure 5: Time evolution of the amount of displaced output strand (in pmol), as a function of the initial amount of M13mp18 virus: 0 pmol (red triangles), 1 pmol (blue squares), 2 pmol (black circles). For each of these three experiments, we successively considered: addition of the input and fuel activator ($0 \text{ s} < t < 1500 \text{ s}$), addition of I_{act}^5 .

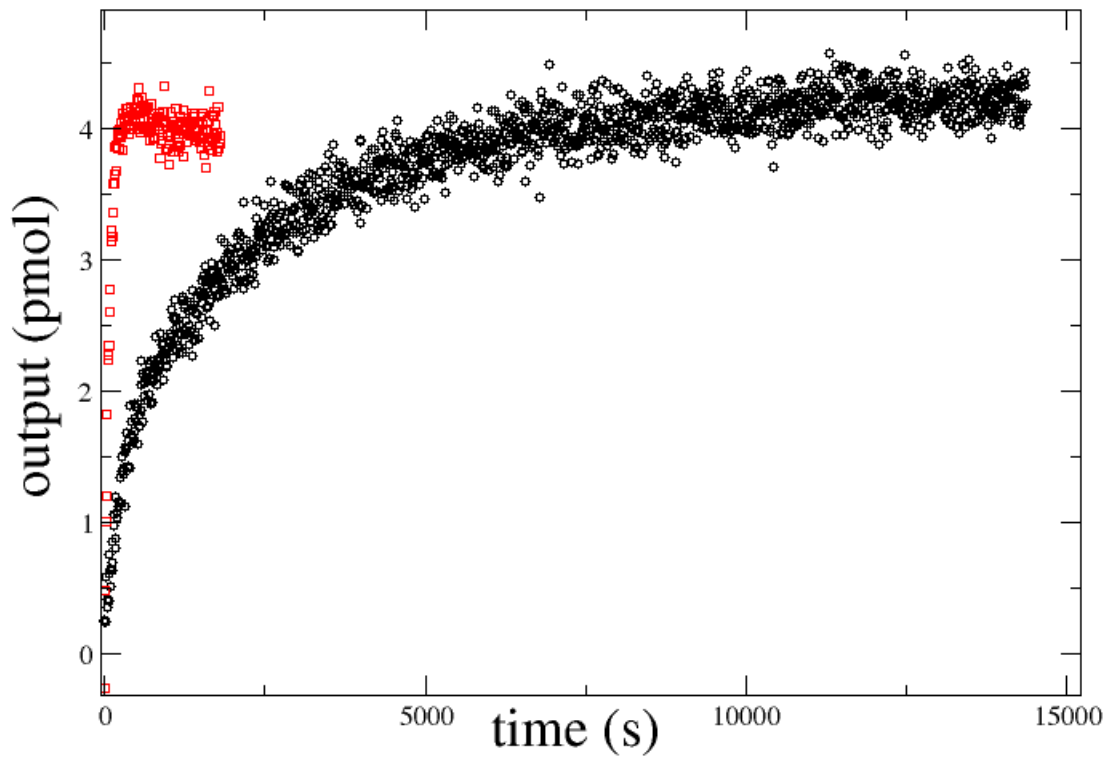


Figure 6: Influence of the tethering on the dynamics: the fastest dynamics corresponds to the tethered system (red squares), the bulk system is represented with black circles. Both experiments have the same initial concentration of input (4nM), gate (16nM) and fuel strands (16nM), and were activated with the same concentration (100nM) of activator strand.

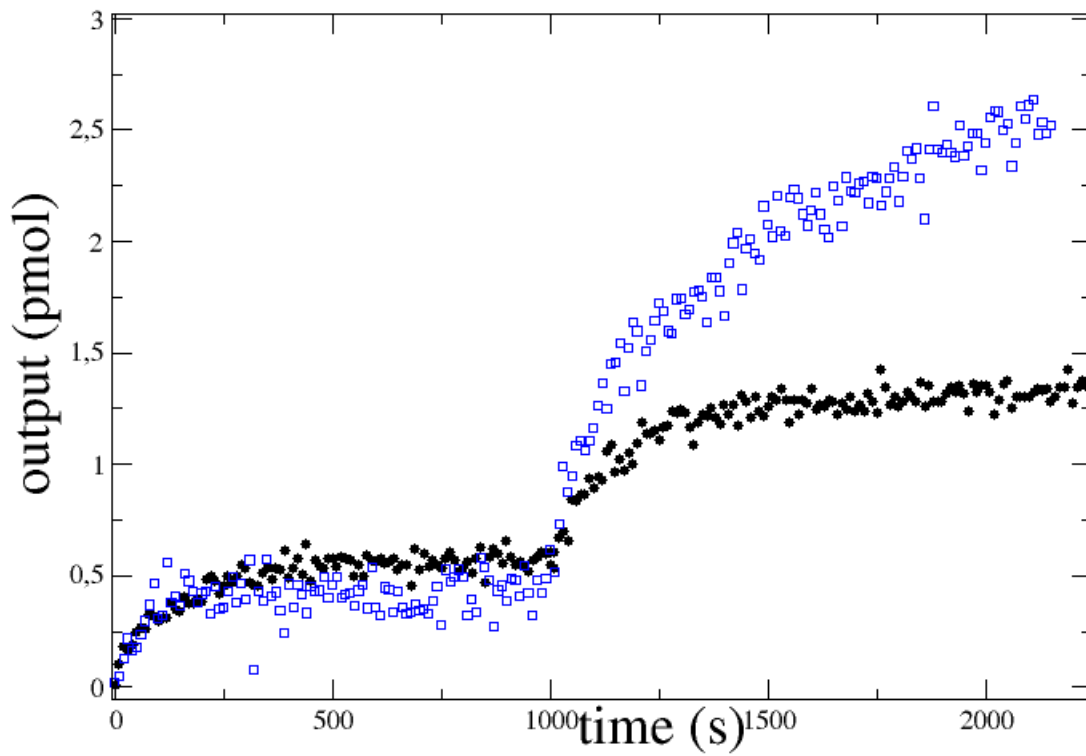


Figure 7: Comparison between the asymmetric (empty squares) and symmetric (black circles) systems. The input is activated at the beginning of the dynamics ($t=0$ s), the fuel is activated at $t = 1000$ s. The asymmetric system looks similar to the expected 1:3 behaviour.